Chemosphere 211 (2018) 573–583

Contents lists available at ScienceDirect

Chemosphere

journal homepage: www.elsevier.com/locate/chemosphere

Antioxidative response of *Phanerochaete chrysosporium* against silver nanoparticle-induced toxicity and its potential mechanism

Zhenzhen Huang [a, 1], Kai He [a, 1], Zhongxian Song [b, 1], Guangming Zeng [a, *], Anwei Chen [c, **], Lei Yuan [a], Hui Li [a], Liang Hu [a], Zhi Guo [a], Guiqiu Chen [a]

[a] *College of Environmental Science and Engineering, Hunan University and Key Laboratory of Environmental Biology and Pollution Control (Hunan University), Ministry of Education, Changsha, 410082, PR China*
[b] *Faculty of Environmental and Municipal Engineering, Henan Province Key Laboratory of Water Pollution Control and Rehabilitation Technology, Henan University of Urban Construction, Pingdingshan, 467036, PR China*
[c] *College of Resources and Environment, Hunan Agricultural University, Changsha, 410128, PR China*

HIGHLIGHTS

- Lipid peroxidation was alleviated via enhancement of SOD, CAT, and POD activities.
- POD played a predominant role in effective protection against chronic cell damage.
- Suppression of ROS production was closely related to the depletion of GSH at 24 h.
- HAADF-STEM and EDX analyses revealed particle-specific toxicity mechanism of AgNPs.

GRAPHICAL ABSTRACT

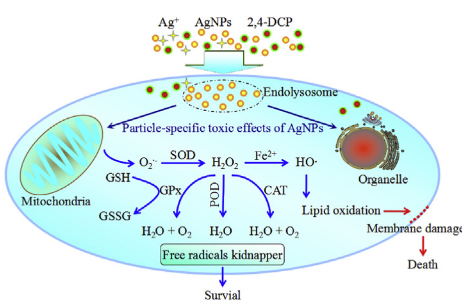

ARTICLE INFO

Article history:
Received 11 May 2018
Received in revised form
30 July 2018
Accepted 31 July 2018
Available online 2 August 2018

Handling Editor: Willie Peijnenburg

Keywords:
Antioxidative enzymes
Oxidative stress
Phanerochaete chrysosporium
Silver nanoparticles
"Particle-specific" effects

ABSTRACT

Antioxidative response of *Phanerochaete chrysosporium* induced by silver nanoparticles (AgNPs) and their toxicity mechanisms were comprehensively investigated in a complex system with 2,4-dichlorophenol (2,4-DCP) and Ag^+. Malondialdehyde content was elevated by 2,4-DCP, AgNPs, and/or Ag^+ in concentration- and time-dependent manners within 24 h, indicating an increase in lipid peroxidation. However, beyond 48 h of exposure, lipid peroxidation was alleviated by upregulation of intracellular protein production and enhancement in the activities of superoxide dismutase (SOD), catalase (CAT), and peroxidase (POD). Comparatively, POD played more major roles in cell protection against oxidative damage. Furthermore, the dynamic change in reactive oxygen species (ROS) level was parallel to that of oxidized glutathione (GSSG), and ROS levels correlated well with GSSG contents ($R^2 = 0.953$) after exposure to AgNPs for 24 h. This finding suggested that elimination of oxidative stress resulted in depletion of reduced glutathione. Coupled with the analyses of anoxidative responses of *P. chrysosporium* under the single and combined treatments of AgNPs and Ag^+, HAADF-STEM, SEM, and EDX demonstrated that AgNP-induced cytotoxicity could originate from the original AgNPs, rather than dissolved Ag^+ or the biosynthesized AgNPs.

* Corresponding author.
** Corresponding author.
E-mail addresses: zgming@hnu.edu.cn (G. Zeng), A.Chen@hunau.edu.cn (A. Chen).

[1] These authors contribute equally to this article.

https://doi.org/10.1016/j.chemosphere.2018.07.192
0045-6535/

1. Introduction

Nanomaterials are defined as supramolecular compounds with at least one dimension less than 100 nm that possess peculiar physicochemical properties; they have been rapidly expanding applications in biology, medicine, and biochemical engineering (Shi et al., 2014; Xu et al., 2012; Gong et al., 2009; Lin et al., 2008). Metallic silver nanoparticles (AgNPs) are the most extensively used nanomaterial because of their potent and broad-spectrum antibacterial, antifungal, and antiviral activities (Wang et al., 2012; Windler et al., 2013). Given the explosion in the use of silver nanotechnology, AgNPs have inevitably been released into industrial and domestic effluent streams directly or through discharges of municipal wastewater, leading to accumulation, transformation, and degradation in the atmosphere, water, soil, or organisms (Das et al., 2012; Liu et al., 2014; Sheng and Liu, 2011; Zeng et al., 2013a). AgNPs have been proven to be a potential threat to environments, especially aquatic environments, because of their relatively high toxicity toward some aquatic organisms and microbial communities in biological treatment processes (Liu and Hurt, 2010; Borm and Berube, 2008; Feng et al., 2010).

A myriad of studies have shown that the toxic effect of AgNPs is primarily attributed to the released Ag^+. Blaser et al. (2008) found that 15% of the total Ag from Ag-based products was released into water when analyzing the risk of releasing AgNPs into the ecosystem. It is well known that the Ag^+ can inactivate bacterial cell electron transport, ATP production, and DNA replication and it can interact with thiol groups in enzymes, causing cells to be in a nonculturable state and even leading to cell death (Massarsky et al., 2013; Morones et al., 2005). Furthermore, AgNPs, which have been documented to readily penetrate through biological barriers and cell membranes (AshaRani et al., 2009), interfere with specific biological systems and cellular functions including permeability and respiration (Morones et al., 2005; Fröhlich, 2013; Foldbjerg et al., 2011). Reactive oxygen species (ROS) generation was stimulated, and antioxidant defense system elements were suppressed under AgNP stress. These effects resulted in serious cellular damage, degradation of the membrane structures of cells, protein and lipid peroxidation, and DNA breaks, either directly or indirectly (Krawczyńska et al., 2015; Jones et al., 2011; Yildirimer et al., 2011; Kim and Ryu, 2013; Zeng et al., 2013b). Regarding the extended release of a large amount of Ag^+ and differences in antimicrobial mechanisms of Ag^+ and AgNPs, influences of coexistence of AgNPs and Ag^+ on evaluation of the ecotoxicity of AgNPs cannot be ignored. Although synergism or antagonism of combinations of AgNPs and Ag^+ on the number of cells and growth rates in *Escherichia coli* have been reported (Choi et al., 2018), whether the combined toxic effects mainly originated from the "particle-specific" antimicrobial activity of AgNPs remains an open question (Xiu et al., 2012). Furthermore, AgNPs have been widely used for monitoring, adsorption, photocatalytic degradation of various water contaminants such as cadmium (Cd) and 2,4-dichlorophenol (2,4-DCP) (Zuo et al., 2015; Huang et al., 2017). It provides abundant opportunities for the coexistence of AgNPs, Ag^+, and 2,4-DCP in the environment. Our previous studies have found that exposure of AgNPs to *Phanerochaete chrysosporium* (*P. chrysosporium*) can greatly improve the removal efficiency of Cd(II) and 2,4-DCP (Huang et al., 2017; Zuo et al., 2015). This could be closely associated with the antioxidant defense systems of microorganisms in complex systems with nanomaterials and toxic pollutants.

Antioxidant defense systems are composed of non-enzymatic and enzymatic antioxidants. Non-enzymatic antioxidants include lipid-soluble membrane-associated antioxidants and water-soluble reductants (e.g., ascorbic acid and glutathione). Antioxidative enzymes, including superoxide dismutase (SOD), catalase (CAT), and peroxidase (POD), play critical roles in oxidative stress defense in fungi (Chen et al., 2014; Zhang et al., 2007). Reduced glutathione (GSH), a sulfur-containing tripeptide thiol, could scavenge free radicals or serve as a cofactor for glutathione peroxidase (GPx), oxidizing GSH to diminish H_2O_2. SOD, the first defense line against ROS, converts O_2^- to H_2O_2. Subsequently, H_2O_2 is detoxified by CAT and POD. The enzymatic action of CAT leads to the formation of water and molecular oxygen, while the decomposition of H_2O_2 by POD is achieved by oxidizing co-substrates such as aromatic amines, phenolic compounds, and/or antioxidants (Qiu et al., 2008).

P. chrysosporium, as a model strain of white rot fungi, has been employed to remove organic substrates and heavy metals in wastewater on account of its desirable biodegradation and biosorption ability (Zeng et al., 2012; Huang et al., 2008, 2015). However, how *P. chrysosporium* responds to contamination of aquatic systems with a combination of AgNPs, Ag^+, and toxic organics *in vivo* is unclear. Hence, in order to maximize the promising applications of AgNPs and white rot fungi in bioremediation, it is necessary to understand the bioeffects of AgNPs on the antioxidant system and pertinent biochemical detoxification mechanisms to stress tolerance in a complex system.

The present study therefore focused on the antioxidative responses of *P. chrysosporium*, at the metabolic and physiological levels, following exposure to various concentrations of 2,4-DCP, AgNPs, and Ag^+. Cellular viability, lipid peroxidation, activities of antioxidant enzymes (SOD, CAT, and POD), glutathione levels, and intracellular protein contents were determined using a UV–vis spectrophotometer. ROS generation was also assessed by fluorescence spectrometry. Furthermore, relationships between stress intensities and antioxidant fluctuations, and interactions of various antioxidants with free radicals were evaluated to identify toxicant-induced oxidative damage, antioxidative defense mechanisms of *P. chrysosporium* against these stresses, and approaches of AgNP-evoked cytotoxicity.

2. Materials and methods

2.1. Strain and treatments

P. chrysosporium strain BKMF-1767 (CCTCC AF96007) was obtained from the China Center for Type Culture Collection (Wuhan, China) and maintained on malt extract agar slants at 4 °C. The spore suspension was adjusted to a concentration of 2.0×10^6 CFU/mL by scraping the spores into sterilized ultrapure water, inoculated into the culture medium, and cultivated in an incubator at 37 °C and 150 rpm for 3 days. *P. chrysosporium* pellets were harvested, rinsed three times with 2 mM $NaHCO_3$, and then exposed to four treatment groups: 1) 2,4-DCP-treated groups including a series of 2,4-DCP concentrations (0, 153, 307, and 613 μM) with 10 μM AgNPs; 2) AgNP-treated groups composed of various concentrations of AgNPs (0, 1, 10, 30, 60, and 100 μM) with 153 μM 2,4-DCP; 3) Ag^+-treated groups containing different concentrations of Ag^+ (using $AgNO_3$ as the ion source; 0.01, 0.1, 1, 10, and 100 μM) with 153 μM 2,4-DCP; and 4) a combined treatment of AgNPs and Ag^+ consisting of 10 μM AgNPs, 1 μM Ag^+, and 153 μM 2,4-DCP. Subsequently, fungal pellets were collected from test solutions at pre-decided intervals for the succeeding experiments. Citrate-stabilized AgNPs were used in this work and prepared according to our previous report (Huang et al., 2017). The desired doses of AgNPs were obtained by dilution of the AgNP stock solution with 2 mM $NaHCO_3$ buffer solution (Cheng et al., 2016). Detailed descriptions on synthesis and characterization of AgNPs can be found in Supporting Information (SI).

2.2. Cellular viability and ROS generation

MTT assay was performed to evaluate the metabolic activity of *P. chrysosporium* according to previous studies (Chen et al., 2014; Luo et al., 2013). Absorbance was measured at 534 nm by utilizing a UV–vis spectrophotometer (Model UV-2550, Shimadzu Company, Tokyo, Japan), and the viability of *P. chrysosporium* was expressed as relative percentages to the control. *P. chrysosporium* cells that untreated with 2,4-DCP, AgNPs, and Ag^+ were used as the control.

ROS generation was determined by a FluoroMax-4 fluorescence spectrometer (Horiba Scientific, Tokyo, Japan) with an excitation wavelength of 485 nm and an emission wavelength of 525 nm using the cell permeable indicator, 2′,7′-dichlorodihydrofluorescein diacetate (López et al., 2006). To visualize changes in intracellular ROS, the stained cells were imaged using an Olympus Fluoview 1000 laser scanning confocal microscope (LSCM, Olympus TY1318, Tokyo, Japan) (Yang et al., 2010).

2.3. Lipid peroxidation

Lipid peroxidation was estimated by determining malondialdehyde (MDA) content in *P. chrysosporium*. Samples of 0.2 g of fungal pellets were homogenized in 2.5 mL of 10% tricholoroacetic acid (TCA). 2 mL of the extracts was added into 2 mL of 6% thiobarbituric acid and then absorbance of the mixture was recorded at 532 and 600 nm following the reported procedures (Zeng et al., 2012; Choudhary et al., 2007).

2.4. Antioxidative analyses

For further analysis of antioxidative potential of *P. chrysosporium*, the activities of SOD and CAT were evaluated by following the method described by Qiu et al. (2008); POD activity was tested by monitoring the oxidation of guaiacol (Chen et al., 2014); GSH and total glutathione (tGSH) contents were determined according to Rehman and Anjum (2010). 50% inhibition of the reaction was defined as one unit of SOD activity. One unit of CAT (POD) was defined as decrease (increase) of 0.1 (0.01) unit of A_{240} (A_{470}) per min. The enzyme activities were expressed as U/g FW.

2.5. Mechanism and data analysis

Scanning electron microscope (SEM, FEI, USA) equipped with an energy dispersive x-ray (EDX) was used to measure the surface morphology of the freeze-dried fungal pellets, which were collected from the solutions with single AgNPs (Ag^+) and a combination of AgNPs and Ag^+. After freeze-dried samples were ground to a power, physicochemical transformation of AgNPs under stressed conditions was analyzed by scanning transmission electron microscopy in high-angle annular dark field mode (HAADF-STEM) coupled with an EDX system. X-ray diffraction (XRD, D8 Discover-2500, Bruker, German) of samples was also performed to further identify crystalline phases.

Data are expressed as the means ± standard deviations of triplicate assays. A one-way analysis of variance (ANOVA) was conducted to test for significant differences ($p < 0.05$) between the experimental groups.

3. Results and discussion

3.1. Characteristics of AgNP suspensions

The as-prepared AgNPs, with an average hydrodynamic diameter of 22.6 ± 2.5 nm and a negative ζ-potential of −11.4 ± 1.1 mV, displayed narrow and intense absorption bands with λ_{max} at 394 nm (Fig. S1). AgNP suspensions containing 2,4-DCP remained relatively high stability with little aggregation and dissolution in comparison to AgNP stock solution (Fig. S1). This could be associated with 2,4-DCP in the solutions, which possibly adsorbed onto the surface of AgNPs and restrained AgNP dissolution. Details are available in the SI (in section *2.1*).

3.2. Viability of P. chrysosporium

As seen in Fig. S3, *P. chrysosporium* survival was stimulated by low-dose AgNPs (0–10 μM), Ag^+ (0.01–1 μM) and 2,4-DCP (153 μM); however, high concentrations of AgNPs (≥100 μM), Ag^+ (≥10 μM), and 2,4-DCP (≥307 μM) exhibited a striking cytotoxicity, and *P. chrysosporium* appeared much more susceptible to Ag^+ than AgNPs. Although an apparent inhibition following exposure to high-dose AgNPs and 2,4-DCP was observed, Ag^+ release from AgNPs for all tested treatments with AgNPs and 2,4-DCP has been well documented at very low levels, much less than 1 μM (Huang et al., 2017). The findings revealed that significant inhibitory effects could be triggered by high-level exposure to toxicants, rather than by the released Ag^+ in the aqueous solutions. Details on cellular viability are provided in the SI (in section *2.2*).

Cellular viability after the combined treatment with 10 μM AgNPs and 1 μM Ag^+ was appreciably lower than that in each treatment alone. The most likely reason was that Ag^+ absorbed onto AgNP surface or formed complexes with the citrate coating on AgNPs through electrostatic attraction, leading to AgNPs surrounded by a "cloud" of Ag^+ (Liu and Hurt, 2010; Huynh et al., 2014), which could also cause the lower dissolution of AgNPs. Thus, the concentration of Ag^+ surrounding AgNPs was comparatively higher than that in the bulk solution. When AgNPs attached to or came into close proximity with the fungal membranes, the fungi would be exposed to a considerably higher Ag^+ concentration, leading to inactivation of the *P. chrysosporium* cells.

3.3. ROS generation

To illustrate oxidative responses of *P. chrysosporium* to AgNPs, Ag^+, and 2,4-DCP, intracellular ROS generation was evaluated after 24-h stimulation with these toxicants. A distinct increase in ROS levels was observed after treatment with low-dose AgNPs (especially for 1 μM); however, ROS production, induced by high concentrations of AgNPs, decreased in a dose-dependent manner, to even lower levels than that of the control (Fig. 1A). Similarly, ROS generation in the Ag^+- and 2,4-DCP-treated groups was noticeably stimulated at exposure concentrations of 0.01, 0.1, and 1 μM Ag^+, and 153 μM 2,4-DCP, but a contrary concentration-related pattern was observed at high levels of Ag^+ and 2,4-DCP (Fig. 1B and C). It is not unusual for oxidative effects to be more severe at lower exposure concentrations (Choi et al., 2010). This could be accounted for by the fact that ROS were primarily generated as a natural byproduct during the process of normal aerobic metabolism in mitochondria, the functions of which might be disrupted after the occurrence of ROS formation or reaching its detectable level (Chen et al., 2014). Besides, the drastic reduction in the ROS levels for high-concentration exposure could be explained by the fact that irreparable metabolic dysfunction and apoptosis (programmed cell death) were evoked by oxidative stress (Zeng et al., 2012), resulting in a diminution in the cell concentration, as depicted in the cell viability assay (Fig. S3).

ROS levels induced by the combination of 10 μM AgNPs and 1 μM Ag^+ were insignificantly different from those triggered by either 10 μM AgNPs or 1 μM Ag^+, but much higher than that in cells subjected to only 10 μM Ag^+ (Fig. 1A and B). This indicated that

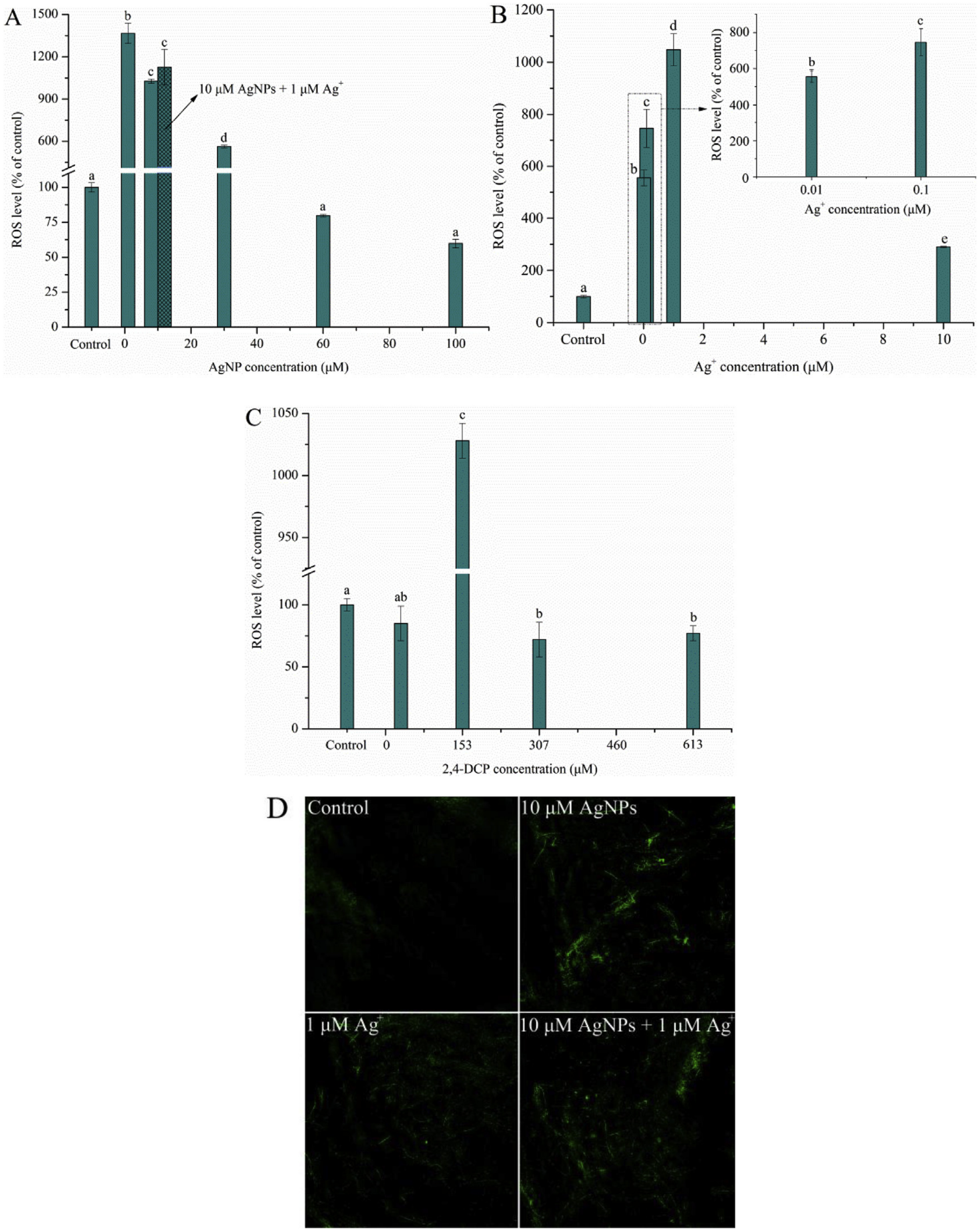

Fig. 1. ROS level after treatment with various doses of (A) AgNPs, (B) Ag^+, and (C) 2,4-DCP for 24 h; (D) LSCM images for ROS production.

based on total Ag concentration, Ag^+ ions were more toxic to *P. chrysosporium* than AgNPs, resulting in the population not easily recovering from Ag^+ exposure. Furthermore, as aforementioned, AgNPs can be surrounded by a "cloud" of Ag^+ due to Ag^+ adsorption and complexation. With the addition of exogenous Ag^+, more Ag^+ ions will be adsorbed on AgNP surface. The attachment or close proximity of AgNPs to cell membranes could enhance the locally high Ag^+ concentration at the nanoparticle-cell interface and accumulation of AgNPs in cell membranes might also induce local disruption of the bilayer structure and affect the lipid bilayer phase behavior (Häffner and Malmsten, 2017). However, changes in ROS levels and cellular viability under stress of AgNP and Ag^+, separately or in combination, indicated that low-dose AgNP/Ag^+-induced cell damage was deemed to be recoverable. Additionally, the pattern of dose-related ROS generation was also verified by LSCM images (Fig. 1D and S4), which showed higher-intensity fluorescence at lower exposure concentrations.

3.4. Lipid peroxidation

A dose-dependent increase in MDA content was found in *P. chrysosporium* after 2-h exposure to 2,4-DCP (Fig. 2A), suggesting concentration-dependent stimulation in imposed lipid peroxidation of the cell membrane and other organelles (Chen et al., 2014). The stimulation was initiated at low concentrations (0–307 μM). On further increasing the concentration to 613 μM, however, the

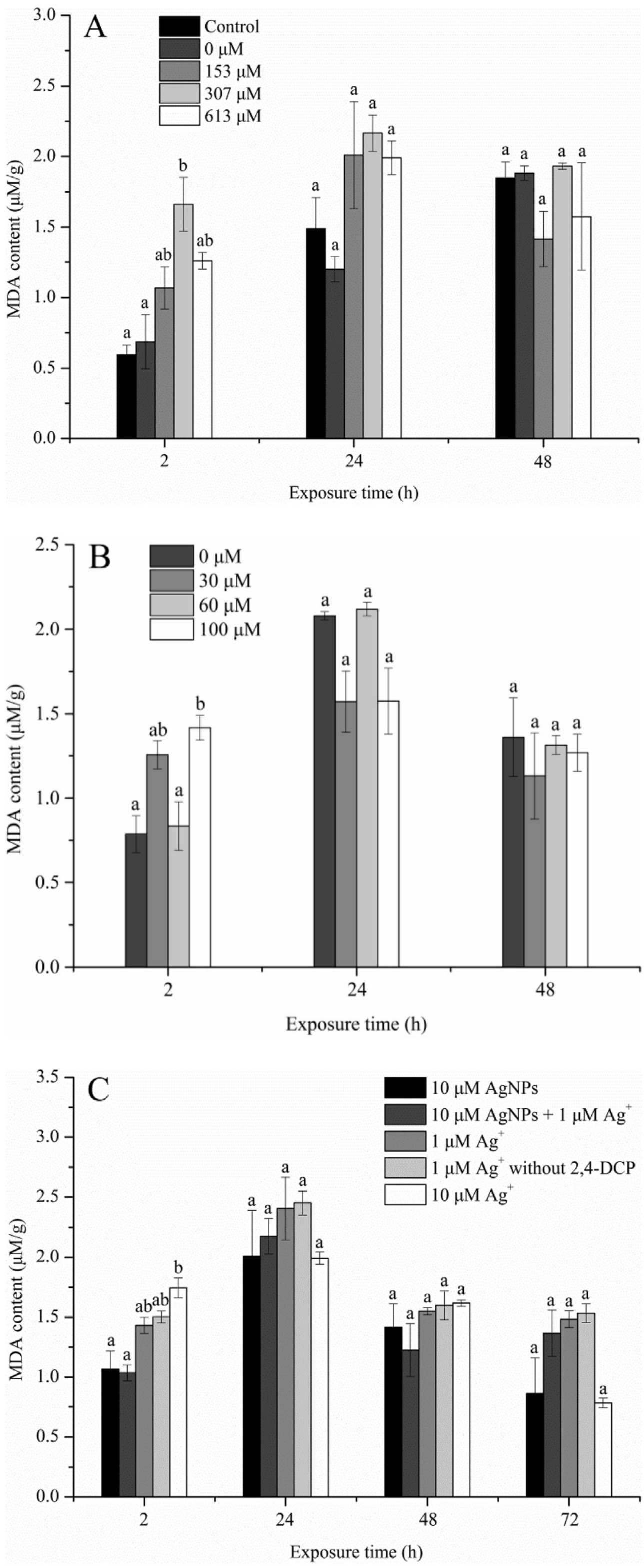

Fig. 2. MDA content upon the administration of (A) 2,4-DCP, (B) AgNPs, and (C) Ag^+ and AgNPs + Ag^+ for 2–72 h.

MDA content was somewhat suppressed. Coupled with the cell viability results (Fig. S3C), high concentrations of 2,4-DCP led to cell necrosis or death, causing the release of MDA from these cells (Jiang et al., 2014). It was also observed that although 2,4-DCP concentrations had no pronounced difference in their effects on membrane lipid peroxidation after 24–48 h, higher MDA levels were elicited by 2,4-DCP treatments for 24 and 48 h than those for 2 h, indicating that 2,4-DCP induced the oxidative stress in the fungal cells due to prolonged exposure.

It has been demonstrated that lipid peroxidation was induced by AgNPs in zebrafish liver, green algae, and higher plants (Choi et al., 2010; Jiang et al., 2014; Oukarroum et al., 2012). In this study, AgNPs dramatically enhanced MDA accumulation to a concentration of 100 μM in 2 h and the highest concentration of MDA was found after 24 h of exposure (Fig. 2B). Nevertheless, a decrease was observed with a further increase in exposure time to 48 h. It could be postulated that free radicals were possibly neutralized by the antioxidative effect of *P. chrysosporium*, resulting in the low detected levels of MDA. To test this hypothesis, quantification of antioxidants was performed. Changes in MDA content showed a similar trend after treatment with Ag^+ and with the AgNPs and Ag^+ complex (Fig. 2C). According to comparative treatments of 1 μM Ag^+ with and without 2,4-DCP, slightly lower MDA levels were detected in the samples with Ag^+ and 2,4-DCP after 2–72 h, suggesting that lipid peroxidation might be alleviated by low concentrations of 2,4-DCP.

3.5. *Antioxidative analyses*

3.5.1. *SOD activity*

Changes in SOD activity in *P. chrysosporium* treated with 2,4-DCP, AgNPs, and Ag^+ were presented in Fig. 3. For short-term exposure (2 h), there was a marked enhancement in SOD activity due to the introduction of 2,4-DCP, whereas, after exposure to 2,4-DCP for 24 h, SOD activity was noted to be lower than that in the control (Fig. 3A). The markedly enhanced SOD activity could be assigned to a direct stimulation of 2,4-DCP on the enzyme activity (Qiu et al., 2008), or the upregulation in the expression of genes encoding SOD when cells respond to compensation of excess superoxide radical (Zeng et al., 2012; Ma et al., 2015). However, the decreasing part in SOD activity at 24 h was considered as an exhaustion phase in which antioxidative defense systems were overloaded, causing chronic damages and even cell death. A similar tendency in SOD level was also observed for a combination treatment of 10 μM AgNPs and 1 μM Ag^+ and Ag^+ treatments with and without 2,4-DCP within 24 h (Fig. 3C). After further exposure to 2,4-DCP, AgNPs, and/or Ag^+ for 48 and 72 h, none of the activities were remarkably different from the control, but an enhancement in SOD activity occurred again when compared with that after 2–24 h of exposure (Fig. 3A–C). This could be associated with the effective removal of these toxicants by *P. chrysosporium* after 48 h (Huang et al., 2017). And the surviving *P. chrysosporium* cells may induce more enzymes against oxidative stress and membrane-damaging lipid peroxidation; in turn, the induced enzymes were conducive to recovery of cellular growth and replication.

A statistically insignificant alteration in SOD level was observed under the tested AgNP concentrations with respect to the control at 24 h (Fig. 3B), while 2,4-DCP and Ag^+ caused a significant lower SOD activity than the control did. The results exhibited that in comparison to AgNPs, SOD activity was more vulnerable to 2,4-DCP and Ag^+. Furthermore, although the activities of SOD under the combinative stress of AgNPs and Ag^+ were lower than those under the stresses of single AgNPs and Ag^+ with and without 2,4-DCP within 24 h significantly or insignificantly (Fig. 3C), it cannot be concluded that a combination of AgNPs and Ag^+ have more adverse

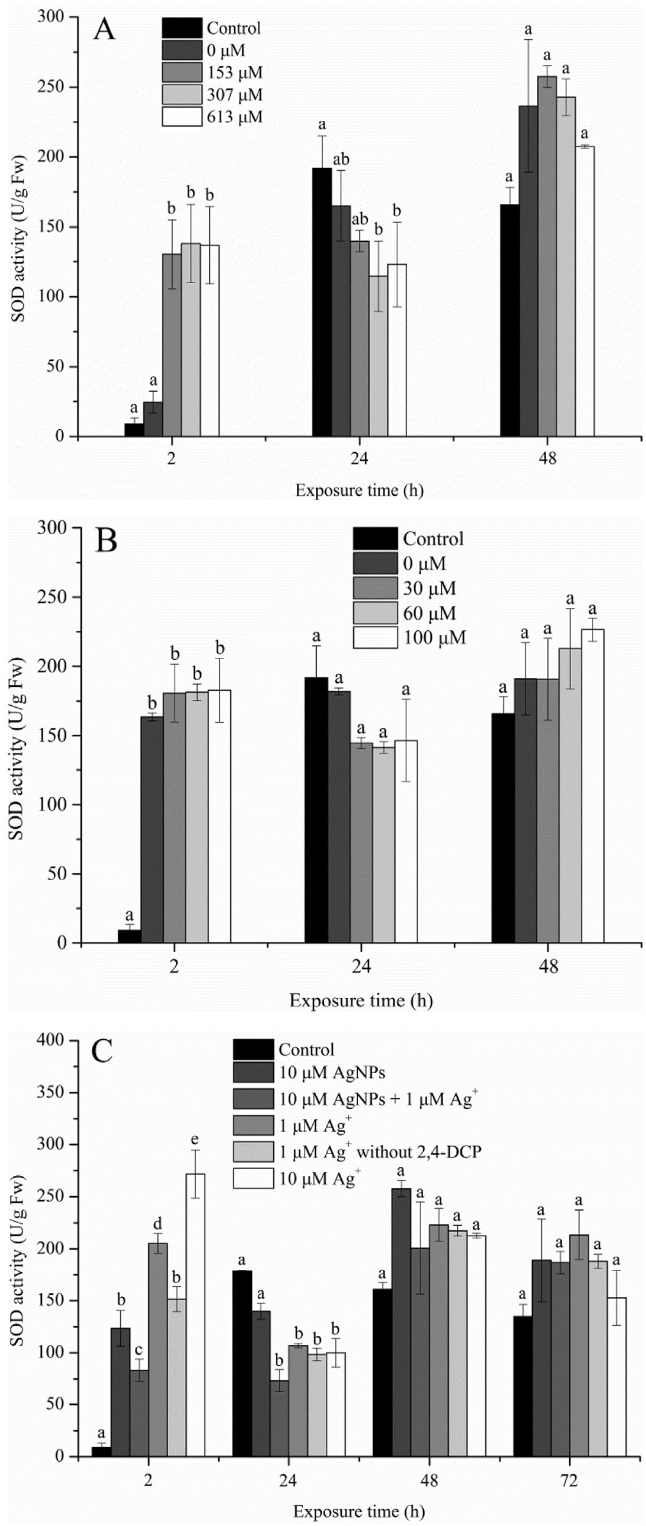

Fig. 3. SOD activity induced by (A) 2,4-DCP, (B) AgNPs, and (C) Ag^+ and AgNPs + Ag^+ after 2–72 h of incubation.

effects on SOD activity than single AgNPs or Ag^+.

3.5.2. CAT activity

CAT, existing in all microorganisms and correlating with microbial activity and respiration, boosts oxidization of compounds by means of H_2O_2. CAT activities were stimulated to a lesser extent when cells were supplemented with 2,4-DCP, AgNPs, and/or Ag^+ for 2 h, and the maximum activity was 57.9 U/g FW in the 10-μM Ag^+ sample (Fig. 4). After 24 h of incubation with these toxicants, various degrees of suppression in CAT activity were noticed, perhaps due to a variety of inhibitory influences of toxicants on subunits assembly or biosynthesis of CAT, or the formation of metal-enzyme complexes, resulting in changing the structure and enzyme activity of CAT (Sun et al., 2009). Specially, CAT activity decreased to non-detectable levels following exposure to 30 and 60 μM AgNPs for 24 h (Fig. 4B). Another possibility of the phenomenon was that AgNP-induced SOD activity was high throughout the exposure period, and that the catalytic activity of SOD caused H_2O_2 accumulation, leading to the depression of CAT (Nelson et al., 2006; Pacini et al., 2013). When the cells were exposed to low concentrations of 2,4-DCP (≤153 μM), AgNPs (≤30 μM), and/or Ag^+ (≤1 μM) for 48–72 h, CAT activities were enhanced to certain extent in contrast to those for 2–24 h; however, higher concentrations of the toxicants noticeably restrained CAT activity. This finding was consistent with observations in Fig. S3 that 2,4-DCP, AgNPs, and Ag^+ showed the expected toxicity with greater biocidal activity with an increase in dose. It has been addressed that recovery of cellular growth and replication occurred more quickly at lower doses than that at higher doses (Mcquillan et al., 2012). Recovery implied an effective adaptive response of microbes to toxicants, which suggested that more enzymes were produce to repair oxidative damage. If enzyme activity under stressed conditions was still depressed with respect to that of the control, it would take longer time for its activity recovery, or enzyme activities cannot be recovered following high-dose and long-term exposure to toxicants.

Besides, it is well-known that AgNPs can enter into the cells through macropinocytosis and endocytosis (Huang et al., 2018a, b; Huang et al., 2017; Wang et al., 2015). Internalization of AgNPs resulted in *P. chrysosporium* being exposed to a locally high Ag^+ concentration within the small size of cells because of large amounts of Ag^+ surrounding AgNP and its dissolution. It was speculated that the influences of both single AgNPs and a combination of AgNPs and Ag^+ on CAT activity were more serious and more difficult to recovery than those of single Ag^+. However, this is not the case. In this study, CAT activities under single 10 μM AgNP stress and the combined stress of 10 μM AgNPs and 1 μM Ag^+ were enhanced with respect to those of the control, and higher than those under 1 μM Ag^+ treatments with and without 2,4-DCP and 10 μM Ag^+ treatments at 48 and 72 h (Fig. 4C). Differences in CAT activity between treatments of 1 μM Ag^+ with and without 2,4-DCP indicated that CAT activity was reinforced by low-dose 2,4-DCP. A similar case was acquired for POD activity evoked by single AgNPs and Ag^+ (with and without 2,4-DCP), as well as their combination during the same exposure period (in section *3.5.3*, Fig. 5C). The findings not only demonstrated that Ag^+ was indeed more potent than AgNPs, but also highlighted that the dissolved Ag^+ could not be the predominant mechanism underlying AgNP-induced cytotoxicity.

3.5.3. POD activity

Changes in POD activity throughout the process were implicated in development of lignolytic microorganisms and degradation of metabolizable constituents (Serra-Wittling et al., 1995). The tendency of POD was similar to those of SOD and CAT within 24 h of exposure to 2,4-DCP, AgNPs and Ag^+ (Fig. 5A–C). POD activities were enhanced with the increasing levels of 2,4-DCP, AgNPs, and Ag^+ at 2 h, but were significantly inhibited compared to the control after 24 h of exposure. Likewise, an increase in POD induced by 2,4-DCP and AgNPs at 48–72 h coincided with the increase in SOD, and

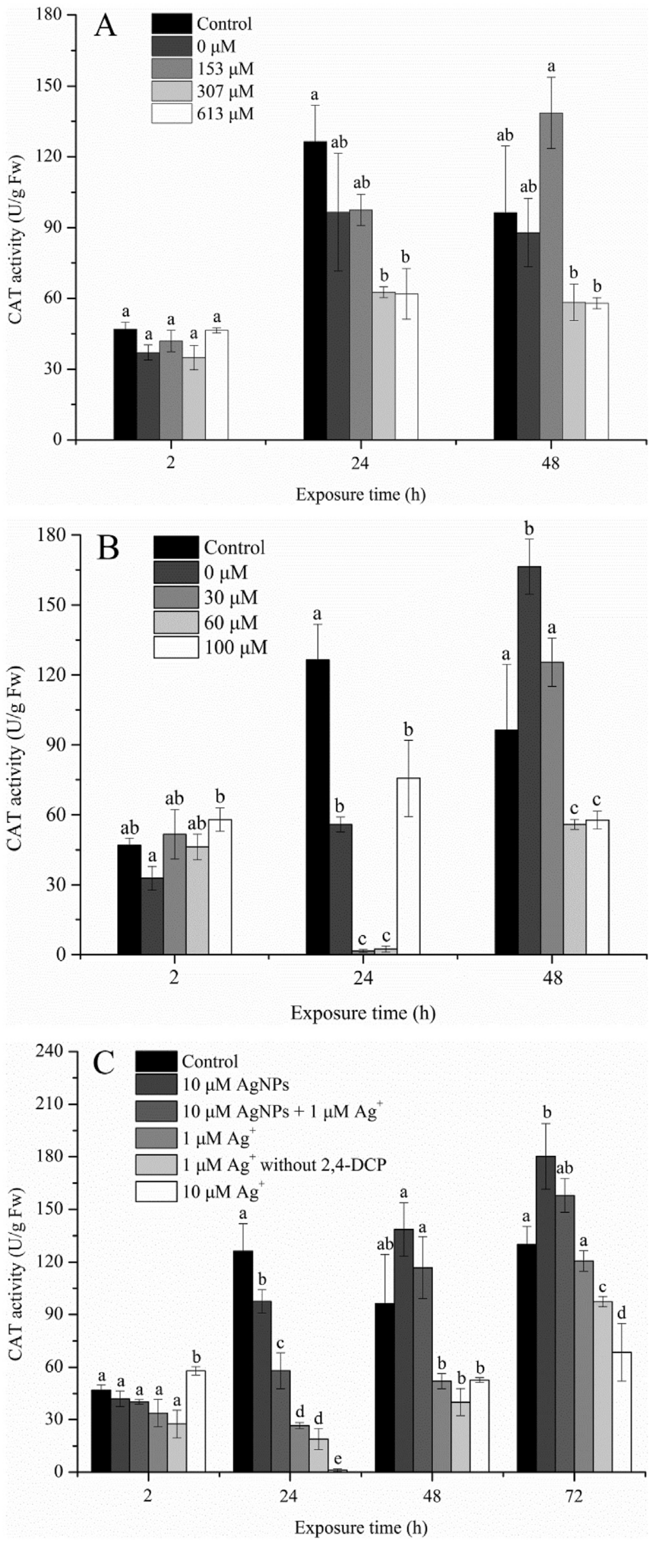

Fig. 4. CAT activity evoked by (A) 2,4-DCP, (B) AgNPs, and (C) Ag^+ and AgNPs + Ag^+ after 2–72 h of exposure.

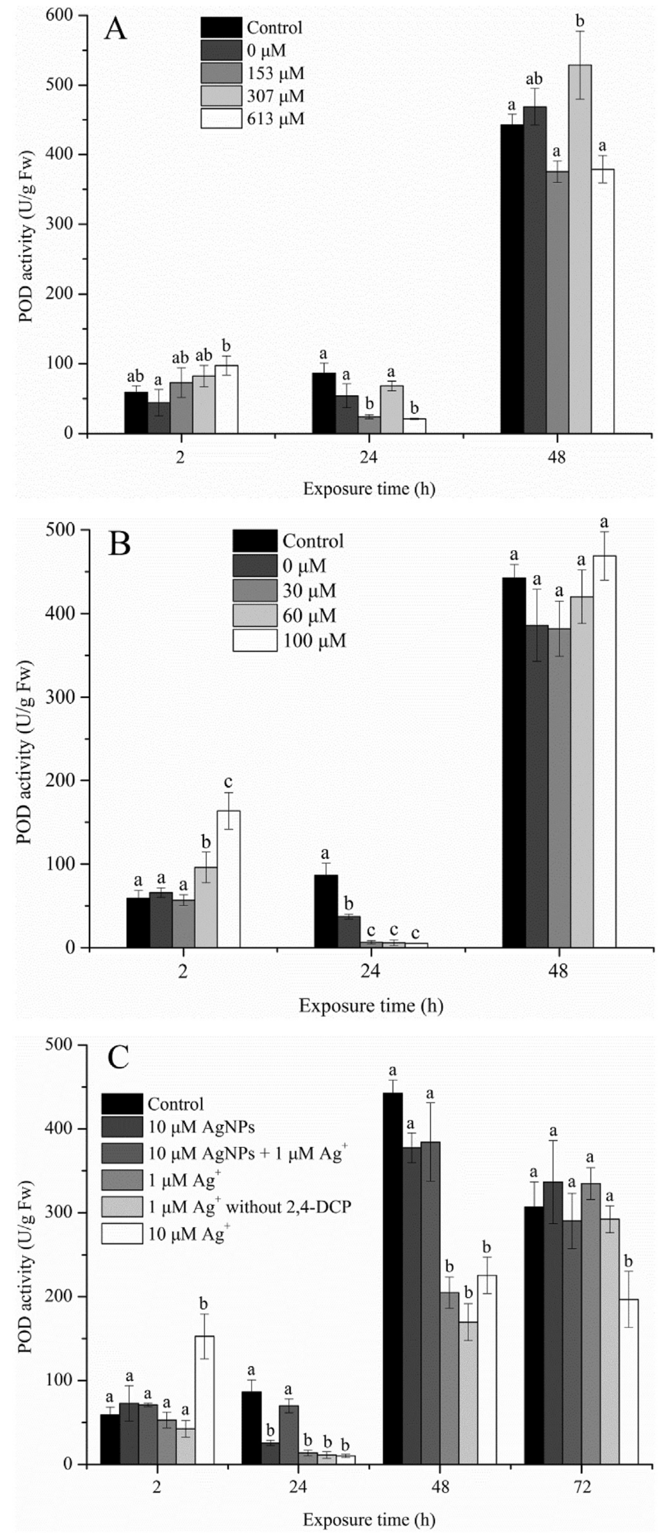

Fig. 5. POD activity under the stress of (A) 2,4-DCP, (B) AgNPs, and (C) Ag^+ and AgNPs + Ag^+ for 2–72 h.

over the same period, the alterations in POD achieved from treatments with Ag^+ (with and without 2,4-DCP) and a combination of AgNPs and Ag^+ were consistent with those in CAT. The prolonged treatment with 2,4-DCP, AgNPs, and Ag^+ induced a sharper increase in POD activities, up to 528.8, 468.8, and 334.6 U/g Fw, respectively, than those in SOD and CAT, the maximum activities of which were 281.4 and 180.2 U/g Fw, respectively. Besides, the distinct difference between POD and CAT after 48–72 h of exposure to 2,4-DCP, AgNPs, and Ag^+ signified that POD was more tolerant to toxicants, playing more important roles in detoxification of H_2O_2 for long-term exposure than CAT doing. Meanwhile, these results indicated that although these three enzyme activities were all at high levels over a long period of exposure, POD exerted the most pronounced influence, protecting *P. chrysosporium* against oxidative stress, chemical toxicity, and certain chronic disorders.

The changing patterns of intracellular proteins in 2,4-DCP, AgNP, and/or Ag^+-treated groups over the exposure time were consistent with those of antioxidative enzymes SOD, CAT, and POD, which further validated the protection of antioxidative enzymes against oxidative damage (Fig. S5). Detailed assessments of intracellular proteins are supplied in the SI (in section *2.3*). Furthermore, the enhancement in free radical-scavenging enzymes (SOD, CAT, and POD) at 48–72 h also corroborated the aforementioned hypothesis that lipid peroxidation for prolonged toxic exposure was relieved to a certain extent by the augmenting antioxidative defense system.

Interestingly, the activities of SOD, CAT and POD were all inhibited when *P. chrysosporium* was exposed to toxicants for 24 h, while cellular viability and ROS levels following low-dose treatments were significantly higher than those of the control. This signified that for short-term exposure, excessive free radicals could be scavenged by non-enzymatic antioxidants, such as glutathione, to protect *P. chrysosporium* against oxidative stress-induced cell damage.

3.5.4. Glutathione

To determine whether glutathione was effective against oxidative damage, the contents of tGSH, GSH, and GSH/oxidized glutathione (GSSG) were assessed in samples treated with 2,4-DCP, AgNPs, and Ag^+. As noted in Fig. 6, the tGSH levels changed little for 2, 48, and 72 h of exposure, except for the case of 30 μM AgNPs at 48 h; however, greater tGSH synthesis was evident in the control and treatments with 0–153 μM 2,4-DCP, 0–60 μM AgNPs, and 1 μM Ag^+ at 24 h. Notably, a drop in tGSH levels was provoked after being exposed to high concentrations of 2,4-DCP, AgNPs, and Ag^+ for 24 h compared to levels in the control. Meanwhile, the overall GSH levels were low and remained almost unchanged, probably because toxicants impeded the generation of GSH-synthesizing enzymes, such as glutamate-cysteine ligase catalytic subunit and GSH synthetase (Piao et al., 2011). Thus, the GSSG content, which was calculated by subtracting GSH from tGSH, was relatively high at low toxicant concentrations and diminished with increasing doses of toxicants. These results led to an increase in GSH/GSSG ratios, the rates of which were faster at higher concentrations of toxicants than those at lower exposure concentrations. In addition, the high GSSG contents obtained at 24 h suggested that depletion of GSH in the reaction of ROS predominantly occurred over this period. Besides, linear analyses of tGSH, GSSG, and ROS levels were performed under AgNP stress (Fig. S6). ROS, tGSH, and GSSG levels were well correlated with AgNP concentrations ($R^2 = 0.961$, 0.991, and 0.965, respectively), and significant correlations between tGSH, GSSG contents, and ROS levels ($R^2 = 0.861$ and 0.953, respectively) were also observed. The findings indicated that GSH depletion indeed played important roles in detoxification of oxidative stress and the potential of *P. chrysosporium* to toxicant tolerance. Our results agreed with the findings of Ma et al. (2015) who reported the involvement of glutathione in AgNP detoxification in *Crambe abyssinica*. Details are provided in SI (in section *2.4*).

Further information can be obtained at 24 h. There was no visible difference in tGSH amount between the treatments of single 10 μM AgNPs and 1 μM Ag^+ (Fig. 6C). However, tGSH contents under combined treatments of AgNPs and Ag^+ were strikingly lower than those under single AgNPs or Ag^+ stress. The lowest amount of tGSH was achieved in 10 μM Ag^+-incubated cells. According to the aforementioned analysis, surrounding each AgNP, if there was a "cloud" of Ag^+ causing adverse effects on cellular metabolism, a

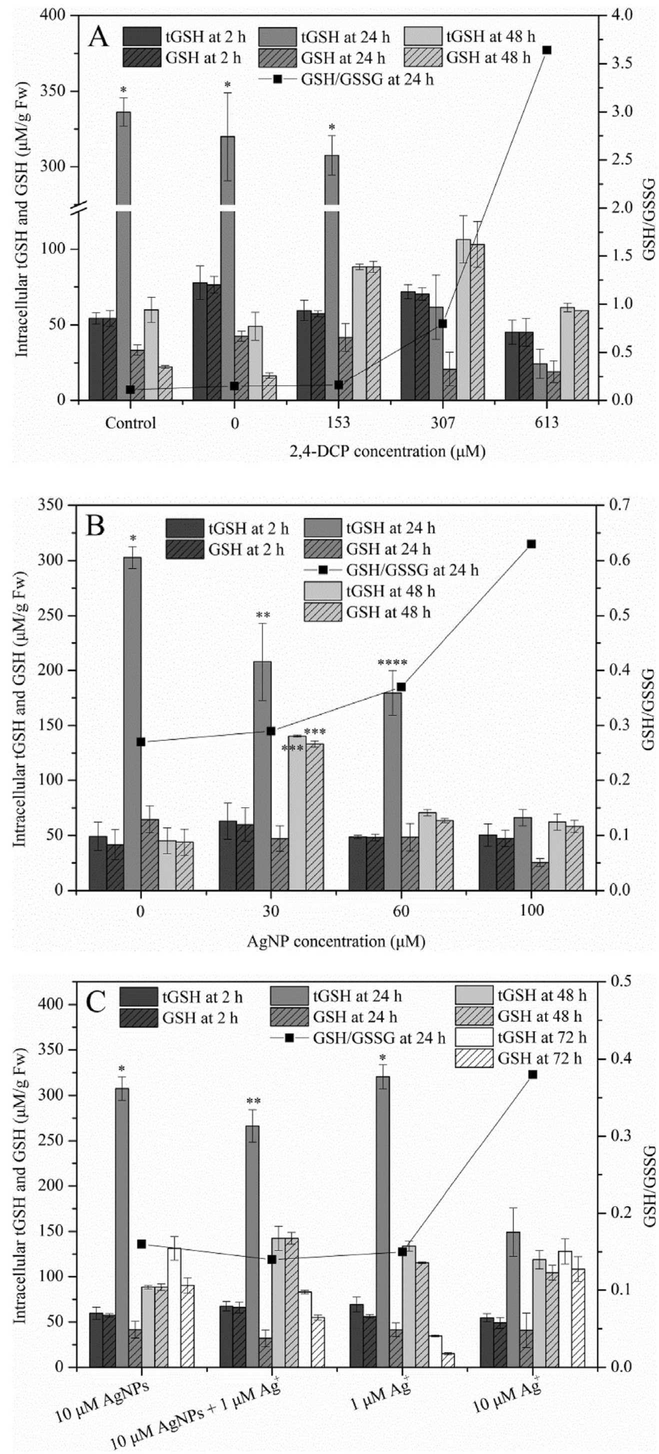

Fig. 6. Alterations of tGSH, GSH, and GSH/GSSG in *P. chrysosporium* exposed to (A) 2,4-DCP, (B) AgNPs, and (C) Ag^+ and AgNPs + Ag^+.

higher tGSH level was not induced by single AgNPs and a combination of AgNPs and Ag^+. These observations further demonstrated that AgNP cytotoxicity might be contributed not by dissolved Ag^+, but by AgNPs themselves.

3.6. Particle-specific toxicity mechanism of AgNPs

In consideration of the analyses of anoxidative responses of SOD, CAT, POD, and glutathione to the single and combined treatments of AgNPs and Ag^{+} in *P. chrysosporium*, AgNP-induced cytotoxicity was proposed presumably through a "particle-specific" pathway, namely, by nanoparticles themselves. To gain further insight into the "particle-specific" toxicity mechanism of AgNPs, freeze-dried fungal pellets from samples treated with 10 μM AgNPs, 1 and 10 μM Ag^{+}, and a combination of 10 μM AgNPs and 1 μM Ag^{+} were analyzed by HAADF-STEM and EDX.

Spherical nanoparticles (bright dots) with diameters of approximately 10–20 nm were observed in samples dosed with AgNPs alone and the combination of AgNPs and Ag^{+} (Fig. 7A and B), which was roughly in conformity with the size of as-prepared AgNPs (11.9 ± 9.4 nm) previously described (Huang et al., 2017). Although the reduction of Ag^{+} to AgNPs by the reducing sugars, derived from saccharides secreted by *P. chrysosporium,* has been documented (Vigneshwaran et al., 2006), no bright dots were found in the single Ag^{+}-treated samples in the present study (data not shown), ruling out biosynthesis of AgNPs by *P. chrysosporium*. EDX observations further confirmed that the nano-sized bright spots were mainly composed of the Ag element, containing a trace quantity of sulfur and undetectable amount of chlorine (Fig. 7C and D). Clear peaks at 2θ values of 38.1°, which can be indexed to (111) of the cubic crystalline structures of AgNPs, were displayed in the XRD patterns of the mycelium samples (Fig. S7). The reason for the weak peak intensities was that AgNP concentrations in samples were low (Chen et al., 2006).

Moreover, SEM images of the AgNPs/Ag^{+}-treated fungus were obtained to examine whether AgNPs were loaded on the surface of fungal mycelia under the stresses of single 10 μM AgNPs and the combination of 10 μM AgNPs and 1 μM Ag^{+} (Fig. 7E and F). The surface of both samples appeared clean and smooth with void spaces but without adhered particles. However, for the combined

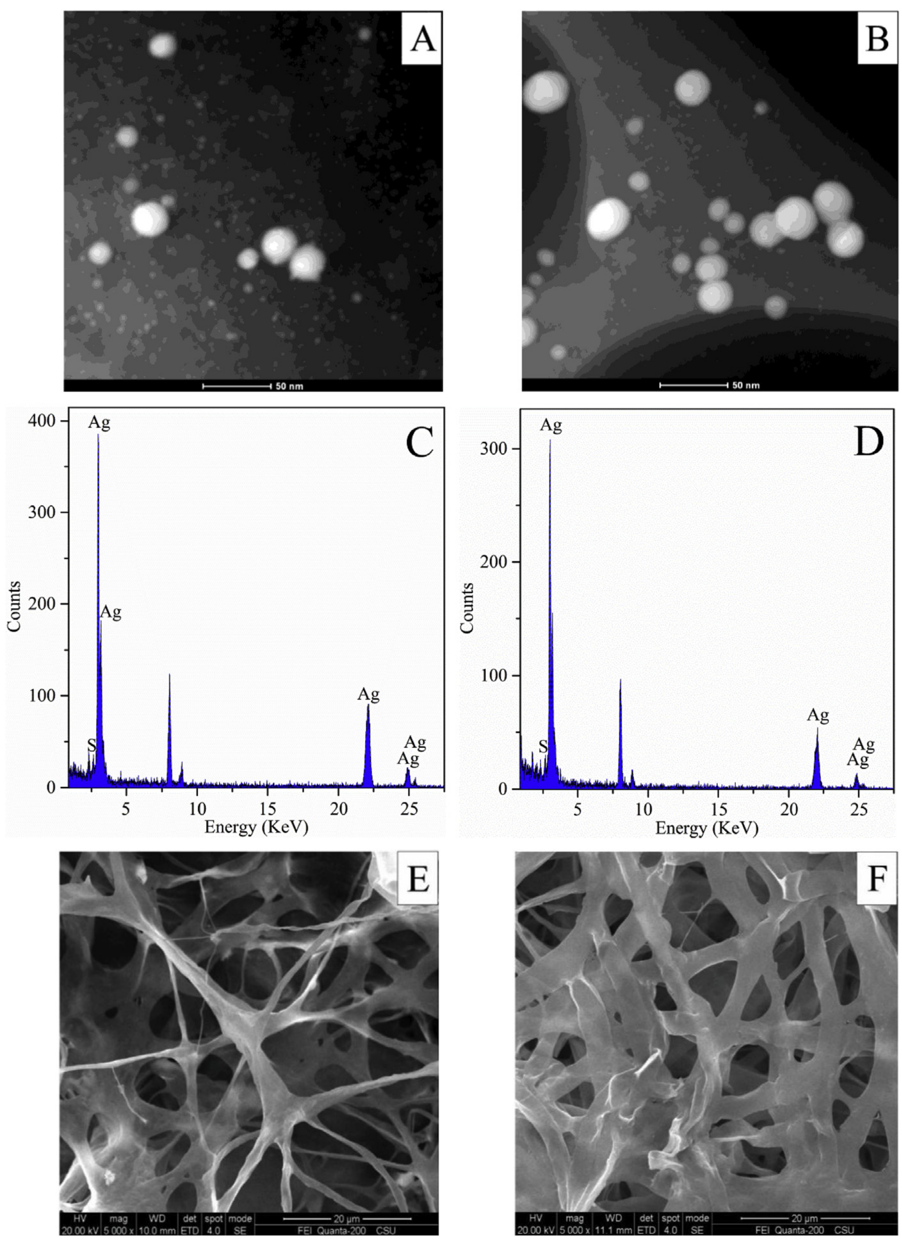

Fig. 7. HAADF-STEM images of freeze-dried fungal pellets from samples exposed to (A) 10 μM AgNPs and (B) 10 μM AgNPs + 1 μM Ag^{+}; (C) and (D) EDX spectra of the bright spots appearing in (A) and (B), respectively; SEM micrographs of the surface of samples treated with (E) 10 μM AgNPs and (F) 10 μM AgNPs + 1 μM Ag^{+}.

treatment of AgNPs and Ag^+, widened and tight mycelia were observed (Fig. 7F), indicating that Ag^+ addition indeed caused changes in the morphological characteristics of *P. chrysosporium*. This was in accordance with the above-mentioned observation regarding cellular viability. Besides, the EDX spectra were also used to analyze the elemental composition of fungal mycelia as indicated in Fig. S8A and B. Negligible peaks corresponding to Ag suggested only a small amount of Ag being absorbed onto the surface of the biomass.

Collectively, it could be ascertained that AgNPs were directly taken up into the cells and AgNP toxicity to *P. chrysosporium* primarily originated from the original AgNPs via “particle-specific” effects, excluding dissolved Ag^+ and the biosynthesized AgNPs.

4. Conclusions

In the present study, lipid peroxidation was alleviated at 48–72 h via improvement of SOD, CAT, and POD activities, and upregulation of proteins production. ROS levels were well correlated with GSSG contents after 24-h AgNP treatments, suggesting that depletion of GSH contributed to suppression of ROS generation. Coupled with antioxidative responses under the single and combined stresses of AgNPs and Ag^+, HAADF-STEM, SEM and EDX observations revealed the “particle-specific” toxicity of AgNPs to *P. chrysosporium*. Results from this work may be utilized to advance the mechanistic understanding of the fungal toxicity mediated by toxicants and the pathways by which AgNPs exert cytotoxicity against microorganisms in complex systems.

Acknowledgements

This work was financially supported by the National Natural Science Foundation of China (51579099, 51521006 and 51508186), the Program for Changjiang Scholars and Innovative Research Team in University (IRT-13R17), and the Hunan Provincial Natural Science Foundation of China (2016JJ3076).

Appendix A. Supplementary data

Supplementary data related to this article can be found at https://doi.org/10.1016/j.chemosphere.2018.07.192.

References

AshaRani, P.V., Low Kah Mun, G., Hande, M.P., Valiyaveettil, S., 2009. Cytotoxicity and genotoxicity of silver nanoparticles in human cells. ACS Nano 3 (2), 279–290.
Blaser, S.A., Scheringer, M., Macleod, M., Hungerbuhler, K., 2008. Estimation of cumulative aquatic exposure and risk due to silver: contribution of nano-functionalized plastics and textiles. Sci. Total Environ. 390 (2–3), 396–409.
Borm, P.J.A., Berube, D., 2008. A tale of opportunities, uncertainties, and risks. Nano Today 3 (1), 56–59.
Chen, A., Zeng, G., Chen, G., Liu, L., Shang, C., Hu, X., Lu, L., Chen, M., Zhou, Y., Zhang, Q., 2014. Plasma membrane behavior, oxidative damage, and defense mechanism in *Phanerochaete chrysosporium* under cadmium stress. Process Biochem. 49 (4), 589–598.
Chen, M., Wang, L.Y., Han, J.T., Zhang, J.Y., Li, Z.Y., Qian, D.J., 2006. Preparation and study of polyacryamide-stabilized silver nanoparticles through a one-pot process. J. Phys. Chem. B 110 (23), 11224–11231.
Cheng, Y., He, H.J., Yang, C.P., Zeng, G.M., Li, X., Chen, H., Yu, G.L., 2016. Challenges and solutions for biofiltration of hydrophobic volatile organic compounds. Biotechnol. Adv. 34, 1091–1102.
Choi, Y., Kim, H.A., Kim, K.W., Lee, B.T., 2018. Comparative toxicity of silver nanoparticles and silver ions to *Escherichia coli*. J. Environ. Sci. 66 (4), 50–60.
Choi, J.E., Kim, S., Ahn, J.H., Youn, P., Kang, J.S., Yi, J., Ryu, D.Y., 2010. Induction of oxidative stress and apoptosis by silver nanoparticles in the liver of adult zebrafish. Aquat. Toxicol. 100 (2), 151–159.
Choudhary, M., Jetley, U.K., Khan, M.A., Zutshi, S., Fatma, T., 2007. Effect of heavy metal stress on proline, malondialdehyde, and superoxide dismutase activity in the cyanobacterium *Spirulina platensis*-S5. Ecotoxicol. Environ. Saf. 66 (2), 204–209.
Das, P., Williams, C.J., Fulthorpe, R.R., Hoque, M.E., Metcalfe, C.D., Xenopoulos, M.A., 2012. Changes in bacterial community structure after exposure to silver nanoparticles in natural waters. Environ. Sci. Technol. 46 (16), 9120–9128.
Feng, Y., Gong, J.L., Zeng, G.M., Niu, Q.Y., Zhang, H.Y., Niu, C.G., Deng, J.H., Yan, M., 2010. Adsorption of Cd(II) and Zn(II) from aqueous solutions using magnetic hydroxyapatite nanoparticles as adsorbents. Chem. Eng. J. 162 (2), 487–494.
Foldbjerg, R., Dang, D.A., Autrup, H., 2011. Cytotoxicity and genotoxicity of silver nanoparticles in the human lung cancer cell line, A549. Arch. Toxicol. 85 (7), 743–750.
Fröhlich, E., 2013. Cellular targets and mechanisms in the cytotoxic action of non-biodegradable engineered nanoparticles. Curr. Drug Metabol. 14 (9), 976–988.
Gong, J.L., Wang, B., Zeng, G.M., Yang, C.P., Niu, C.G., Niu, Q.Y., Zhou, W.J., Liang, Y., 2009. Removal of cationic dyes from aqueous solution using magnetic multi-wall carbon nanotube nanocomposite as adsorbent. J. Hazard Mater. 164 (2), 1517–1522.
Häffner, S.M., Malmsten, M., 2017. Membrane interactions and antimicrobial effects of inorganic nanoparticles. Adv. Colloid Interface Sci. 248, 105–128.
Huang, D.L., Zeng, G.M., Feng, C.L., Hu, S., Jiang, X.Y., Tang, L., Su, F.F., Zhang, Y., Zeng, W., Liu, H.L., 2008. Degradation of lead-contaminated lignocellulosic waste by *Phanerochaete chrysosporium* and the reduction of lead toxicity. Environ. Sci. Technol. 42 (13), 4946–4951.
Huang, Z., Chen, G., Zeng, G., Chen, A., Zuo, Y., Guo, Z., Tan, Q., Song, Z., Niu, Q., 2015. Polyvinyl alcohol-immobilized *Phanerochaete chrysosporium* and its application in the bioremediation of composite-polluted wastewater. J. Hazard Mater. 289, 174–183.
Huang, Z., Chen, G., Zeng, G., Guo, Z., He, K., Hu, L., Wu, J., Zhang, L., Zhu, Y., Song, Z., 2017. Toxicity mechanisms and synergies of silver nanoparticles in 2,4-dichlorophenol degradation by *Phanerochaete chrysosporium*. J. Hazard Mater. 321, 37–46.
Huang, Z., Xu, P., Chen, G., Zeng, G., Chen, A., Song, Z., He, K., Yuan, L., Li, H., Hu, L., 2018a. Silver ion-enhanced particle-specific cytotoxicity of silver nanoparticles and effect on the production of extracellular secretions of *Phanerochaete chrysosporium*. Chemosphere 196, 575–584.
Huang, Z., Zeng, Z., Chen, A., Zeng, G., Xiao, R., Xu, P., He, K., Song, Z., Hu, L., Peng, M., Huang, T., Chen, G., 2018b. Differential behaviors of silver nanoparticles and silver ions towards cysteine: bioremediation and toxicity to *Phanerochaete chrysosporium*. Chemosphere 203, 199–208.
Huynh, K.A., McCaffery, J.M., Chen, K.L., 2014. Heteroaggregation reduces antimicrobial activity of silver nanoparticles: evidence for nanoparticle–cell proximity effects. Environ. Sci. Technol. Lett. 1, 361–366.
Jiang, H.S., Qiu, X.N., Li, G.B., Li, W., Yin, L.Y., 2014. Silver nanoparticles induced accumulation of reactive oxygen species and alteration of antioxidant systems in the aquatic plant *Spirodela polyrhiza*. Environ. Toxicol. Chem. 33 (6), 1398–1405.
Jones, A.M., Garg, S., He, D., Pham, A.N., Waite, T.D., 2011. Superoxide-mediated formation and charging of silver nanoparticles. Environ. Sci. Technol. 45 (4), 1428–1434.
Kim, S., Ryu, D.Y., 2013. Silver nanoparticle-induced oxidative stress, genotoxicity and apoptosis in cultured cells and animal tissues. J. Appl. Toxicol. 33 (2), 78–89.
Krawczyńska, A., Dziendzikowska, K., Gromadzka-Ostrowska, J., Lankoff, A., Herman, A.P., Oczkowski, M., Królikowski, T., Wilczak, J., Wojewódzka, M., Kruszewski, M., 2015. Silver and titanium dioxide nanoparticles alter oxidative/inflammatory response and renin–angiotensin system in brain. Food Chem. Toxicol. 85, 96–105.
Lin, T., Zeng, G.M., Shen, G.L., Li, Y.P., Zhang, Y., Huang, D.L., 2008. Rapid detection of picloram in agricultural field samples using a disposable immunomembrane-based electrochemical sensor. Environ. Sci. Technol. 42 (4), 1207–1212.
Liu, J., Hurt, R.H., 2010. Ion release kinetics and particle persistence in aqueous nanosilver colloids. Environ. Sci. Technol. 44 (6), 2169–2175.
Liu, X., Jin, X., Cao, B., Tang, C.Y., 2014. Bactericidal activity of silver nanoparticles in environmentally relevant freshwater matrices: influences of organic matter and chelating agent. J. Environ. Chem. Eng. 2 (1), 525–531.
López, E., Arce, C., Oset-Gasque, M.J., Cañadas, S., González, M.P., 2006. Cadmium induces reactive oxygen species generation and lipid peroxidation in cortical neurons in culture. Free Radical Biol. Med. 40 (6), 940–951.
Luo, Y.H., Wu, S.B., Wei, Y.H., Chen, Y.C., Tsai, M.H., Ho, C.C., Lin, S.Y., Yang, C.S., Lin, P., 2013. Cadmium-based quantum dot induced autophagy formation for cell survival via oxidative stress. Chem. Res. Toxicol. 26 (5), 662–673.
Ma, C., Chhikara, S., Minocha, R., Long, S., Musante, C., White, J.C., Xing, B., Dhankher, O.P., 2015. Reduced silver nanoparticle phytotoxicity in *Crambe abyssinica* with enhanced glutathione production by overexpressing bacterial γ-glutamylcysteine synthase. Environ. Sci. Technol. 49, 10117–10126.
Massarsky, A., Dupuis, L., Taylor, J., Eisa-Beygi, S., Strek, L., Trudeau, V.L., Moon, T.W., 2013. Assessment of nanosilver toxicity during zebrafish (*Danio rerio*) development. Chemosphere 92 (1), 59–66.
Mcquillan, J.S., Infante, H.G., Stokes, E., Shaw, A.M., 2012. Silver nanoparticle enhanced silver ion stress response in *Escherichia coli* K12. Nanotoxicology 6, 857–866.
Morones, J.R., Elechiguerra, J.L., Camacho, A., Holt, K., Kouri, J.B., Ramirez, J.T., Yacaman, M.J., 2005. The bactericidal effect of silver nanoparticles. Nanotechnology 16 (10), 2346–2353.
Nelson, S.K., Bose, S.K., Grunwald, G.K., Myhill, P., McCord, J.M., 2006. The induction of human superoxide dismutase and catalase *in vivo*: a fundamentally new approach to antioxidant therapy. Free Radical Biol. Med. 40 (2), 341–347.

Oukarroum, A., Bras, S., Perreault, F., Popovic, R., 2012. Inhibitory effects of silver nanoparticles in two green algae, *Chlorella vulgaris* and *Dunaliella tertiolecta*. Ecotoxicol. Environ. Saf. 78, 80–85.

Pacini, N., Elia, A.C., Abete, M.C., Dörr, P., Brizio, A.J.M., Gasco, L., Righetti, M., Prearo, M., 2013. Antioxidant response versus selenium accumulation in the liver and kidney of the Siberian sturgeon (*Acipenser baeri*). Chemosphere 93 (10), 2405–2412.

Piao, M.J., Kang, K.A., Lee, I.K., Kim, H.S., Kim, S., Choi, J.Y., Choi, J., Hyun, J.W., 2011. Silver nanoparticles induce oxidative cell damage in human liver cells through inhibition of reduced glutathione and induction of mitochondria-involved apoptosis. Toxicol. Lett. 201 (1), 92–100.

Qiu, R.L., Zhao, X., Tang, Y.T., Yu, F.M., Hu, P.J., 2008. Antioxidative response to Cd in a newly discovered cadmium hyperaccumulator, *Arabis paniculata* F. Chemosphere 74 (1), 6–12.

Rehman, A., Anjum, M.S., 2010. Multiple metal tolerance and biosorption of cadmium by Candida tropicalis isolated from industrial effluents: glutathione as detoxifying agent. Environ. Monit. Assess. 174 (1), 585–595.

Serra-Wittling, C., Houot, S., Barriuso, E., 1995. Soil enzymatic response to addition of municipal solid-waste compost. Biol. Fertil. Soils 20 (4), 226–236.

Sheng, Z., Liu, Y., 2011. Effects of silver nanoparticles on wastewater biofilms. Water Res. 45 (18), 6039–6050.

Shi, J., Sun, X., Zou, X., Zhang, H., 2014. Amino acid-dependent transformations of citrate-coated silver nanoparticles: impact on morphology, stability and toxicity. Toxicol. Lett. 229 (1), 17–24.

Sun, S.Q., He, M., Cao, T., Zhang, Y.C., Han, W., 2009. Response mechanisms of antioxidants in bryophyte (*Hypnum plumaeforme*) under the stress of single or combined Pb and/or Ni. Environ. Monit. Assess. 149 (1), 291–302.

Vigneshwaran, N., Kathe, A.A., Varadarajan, P.V., Nachane, R.P., Balasubramanya, R.H., 2006. Biomimetics of silver nanoparticles by white rot fungus, *Phaenerochaete chrysosporium*. Colloids Surf., B 53 (1), 55–59.

Wang, Y., Westerhoff, P., Hristovski, K.D., 2012. Fate and biological effects of silver, titanium dioxide, and C_{60} (fullerene) nanomaterials during simulated wastewater treatment processes. J. Hazard Mater. 201, 16–22.

Wang, Z., Xia, T., Liu, S., 2015. Mechanisms of nanosilver-induced toxicological effects: more attention should be paid to its sublethal effects. Nanoscale 7 (17), 7470–7481.

Windler, L., Heightx, L., Nowack, B., 2013. Comparative evaluation of antimicrobials for textile applications. Environ. Int. 53, 62–73.

Xiu, Z.M., Zhang, Q.B., Puppala, H.L., Colvin, V.L., Alvarez, P.J.J., 2012. Negligible particle-specific antibacterial activity of silver nanoparticles. Nano Lett. 12 (8), 4271–4275.

Xu, P., Zeng, G.M., Huang, D.L., Feng, C.L., Hu, S., Zhao, M.H., Lai, C., Wei, Z., Huang, C., Xie, G.X., Liu, Z.F., 2012. Use of iron oxide nanomaterials in wastewater treatment: a review. Sci. Total Environ. 424, 1–10.

Yang, C., Chen, H., Zeng, G., Yu, G., Luo, S., 2010. Biomass accumulation and control strategies in gas biofilters. Biotechnol. Adv. 28, 531–540.

Yildirimer, L., Thanh, N.T.K., Loizidou, M., Seifalian, A.M., 2011. Toxicological considerations of clinically applicable nanoparticles. Nano Today 6, 585–607.

Zeng, G., Chen, M., Zeng, Z., 2013a. Shale gas: surface water also at risk. Nature 499 (7457), 154-154.

Zeng, G., Chen, M., Zeng, Z., 2013b. Risks of neonicotinoid pesticides. Science 340 (6139), 1403-1403.

Zeng, G.M., Chen, A.W., Chen, G.Q., Hu, X.J., Guan, S., Shang, C., Lu, L.H., Zou, Z.J., 2012. Responses of *Phanerochaete chrysosporium* to toxic pollutants: physiological flux, oxidative stress, and detoxification. Environ. Sci. Technol. 46 (14), 7818–7825.

Zhang, Y., Zeng, G.M., Tang, L., Huang, D.L., Jiang, X.Y., Chen, Y.N., 2007. A hydroquinone biosensor based on immobilizing laccase to modified core-shell magnetic nanoparticles supported on carbon paste electrode. Biosens. Bioelectron. 22, 2121–2126.

Zuo, Y., Chen, G., Zeng, G., Li, Z., Yan, M., Chen, A., Guo, Z., Huang, Z., Tan, Q., 2015. Transport fate, and stimulating impact of silver nanoparticles on the removal of Cd(II) by *Phanerochaete chrysosporium* in aqueous solutions. J. Hazard Mater. 285, 236–244.